Bioresource Technology 295 (2020) 122258

Contents lists available at ScienceDirect

Bioresource Technology

journal homepage: www.elsevier.com/locate/biortech

Recombinant production and characterization of six novel GH27 and GH36 α-galactosidases from *Penicillium subrubescens* and their synergism with a commercial mannanase during the hydrolysis of lignocellulosic biomass

Nancy Coconi Linares[a], Adiphol Dilokpimol[a], Henrik Stålbrand[b], Miia R. Mäkelä[a,c], Ronald P. de Vries[a,*]

[a] Fungal Physiology, Westerdijk Fungal Biodiversity Institute & Fungal Molecular Physiology, Utrecht University, Uppsalalaan 8, 3584 CT Utrecht, The Netherlands
[b] Department of Biochemistry and Structural Biology, Lund University, PO Box 124, S-221 00 Lund, Sweden
[c] Department of Microbiology, University of Helsinki, P.O. Box 56, Viikinkaari 9, Helsinki, Finland

ARTICLE INFO

Keywords:
α-Galactosidases
Penicillium subrubescens
Galactomannan
Lignocellulosic biomass
Pichia pastoris
Recombinant expression

ABSTRACT

α-Galactosidases are important industrial enzymes for hemicellulosic biomass degradation or modification. In this study, six novel extracellular α-galactosidases from *Penicillium subrubescens* were produced in *Pichia pastoris* and characterized. All α-galactosidases exhibited high affinity to *p*NPαGal, and only AglE was not active towards galacto-oligomers. Especially AglB and AglD released high amounts of galactose from guar gum, carob galactomannan and locust bean, but combining α-galactosidases with an endomannanase dramatically improved galactose release. Structural comparisons to other α-galactosidases and homology modelling showed high sequence similarities, albeit significant differences in mechanisms of productive binding, including discrimination between various galactosides. To our knowledge, this is the first study of such an extensive repertoire of extracellular fungal α-galactosidases, to demonstrate their potential for degradation of galactomannan-rich biomass. These findings contribute to understanding the differences within glycoside hydrolase families, to facilitate the development of new strategies to generate tailor-made enzymes for new industrial bioprocesses.

1. Introduction

Plant polysaccharides are inexpensive and renewable sources used in the bioprocess industry to produce value added-products, such as biofuels and biochemicals (Malgas et al., 2017). Among these polysaccharides, hemicelluloses, including galacto(gluco)-mannan, xylan and xyloglucan, constitute the second most abundant biopolymer present in nature, after cellulose (Zeilinger et al., 1993). However, the distribution of these hemicellulosic polysaccharides in hardwoods (angiosperms), softwoods (gymnosperms) and legume seeds varies greatly. Hardwoods contain xylans as the major hemicellulosic component, whereas softwoods and legume seeds contain mainly galacto (gluco)-mannan, which consists of linear or branched polymers derived from D-mannose, D-galactose, and D-glucose (Aulitto et al., 2018; Song et al., 2018). The most widely used sources of galacto(gluco)-mannan in industry are guar gum and locust bean gum, extracted from the seeds of *Cyamopsis tetragonolobus* and *Ceretonia siliqua*, respectively, which contain distinctive galactose and mannose ratios (Aulitto et al., 2019).

The complete hydrolysis of galactomannan is a complex process that requires the concerted action of several enzymes, especially endomannanases, β-mannosidases, and α-galactosidases (Coconi Linares et al., 2019). Endomannanases cleavage the mannan backbone to produce oligosaccharides of varying lengths, which can be further processed by β-mannosidases and α-galactosidases (Malgas et al., 2015). α-Galactosidases (EC 3.2.1.22) are a large group of *exo*-acting glycoside hydrolases that catalyze the hydrolysis of α-1,6-linked terminal galactose residues from different substrates, such as galacto-oligosaccharides, galactomannans, galactolipids and α-D-fucosides (Katrolia et al., 2014). Based on amino acid sequence homology, α-galactosidases are classified into six glycoside hydrolase (GH) families (GH4, 27, 36, 57, 97 and 110) of the Carbohydrate-Active enZyme (CAZy) database (http://www.cazy.org/) (Lombard et al., 2014). Although the presence and distribution of α-galactosidases differs in plants, bacteria and fungi, a majority of them belong to either GH27 or GH36, which share a common catalytic mechanism and ancestry (Naumoff, 2011, 2004).

Besides applications in plant biomass conversion, α-galactosidases are also used in other important biotechnological and medical applications. Examples of these are enhancing the kraft pulp bleaching for

* Corresponding author.
E-mail address: r.devries@wi.knaw.nl (R.P. de Vries).

https://doi.org/10.1016/j.biortech.2019.122258
Received 30 August 2019; Received in revised form 9 October 2019; Accepted 10 October 2019
Available online 11 October 2019
0960-8524/

the paper industry, the synthesis of galacto-oligosaccharides via transglycosylation, hydrolysis of indigestible oligosaccharides to improve their nutritional utilization and digestibility, as crystallization aids in the conversion of raffinose to sucrose in the sugar industry, medical treatments such as the modification of blood group glycomarkers on erythrocytes, and enzyme replacement therapy for the Fabry's disease (Aulitto et al., 2019; Katrolia et al., 2014). Despite these existing applications, the identification of novel α-galactosidases with different substrate specificities, high catalytic efficiencies, great synergistic capacity, and high production levels, remains a challenge.

Recently, analysis of the genome sequence of the mesophilic filamentous fungus *Penicillium subrubescens* FBCC1632/CBS132785 revealed an extensive repertoire of genes encoding putative enzymes involved in plant biomass degradation (Peng et al., 2017). Among them, 13 candidate α-galactosidases were found in the genome of *P. subrubescens*, which was a higher number than so far observed in the completely sequenced genomes of other ascomycete fungi *Trichoderma reesei* (10 putative α-galactosidases), *Aspergillus niger* (7), *Myceliophthora thermophila* (3), and *Penicillium chrysogenum* (4), which are well-known models to industrial scale production of hydrolytic enzymes (Berka et al., 2011; de Vries et al., 2017; Jourdier et al., 2017; Vesth et al., 2018). Although several filamentous fungi have been described as prolific producers of α-galactosidases, many of them secrete only low levels of galactosidases within a mixture of other unwanted hydrolytic enzymes (Ademark et al., 2001b; Luonteri et al., 1998a; Sinitsyna et al., 2008). Since the yeast *Pichia pastoris* can produce a large amount of commercially relevant enzymes extracellularly (Kamal et al., 2018; Katrolia et al., 2014), this host has major advantages to simplify enzyme production and purification.

In this study, identification of six novel candidate secreted α-galactosidases from *P. subrubescens* belonging to two distinct GH families, GH27 and GH36, was described. The cDNAs from *P. subrubescens* were successfully cloned and heterologously expressed in *P. pastoris*. The enzymes were biochemically characterized, and the specific activities against diverse galacto-oligosaccharides followed by homology modelling analysis were used to provide a comprehensive mechanism of action of these enzymes. Additionally, the synergistic activities of each of the recombinant α-galactosidases (rAGLs) with a commercial mannanase allowed us to evaluate the differences and similarities in their interactions during the conversion of a variety of galactomannan-rich biomass. These results provide new insights on the substrate specificity and synergism of recombinant enzymes during polysaccharide hydrolysis, and suggest potential applications for the enzymes from *P. subrubescens*.

2. Materials and methods

2.1. Bioinformatic analysis and homology modelling

In order to assess the functional capabilities of each putative α-galactosidase identified in the genome of *P. subrubescens*, all amino acid sequences of fungal α-galactosidases from GH27 and GH36 families that have been characterized biochemically against natural or synthetic substrates were obtained from the CAZy database (http://www.cazy.org/), and included in the multiple sequence alignment. The full-length amino acid sequences of the GH27 and GH36 members from selected fungal genomes, all found in the publicly available JGI Genome MycoCosm database (https://genome.jgi.doe.gov/mycocosm/home), were also included in the alignment.

Putative proteins were verified by BLASTP against the non-redundant sequence database (http://www.ncbi.nlm.nih.gov). Two bacterial α-galactosidases were used as an outgroup for the phylogenetic tree of GH27, while three plant α-galactosidases were used as an outgroup for GH36. SignalP v5.0 (http://www.cbs.dtu.dk/services/SignalP/) was used to detect the presence of secretory signal peptides (Almagro Armenteros et al., 2019). The signal peptides were removed from the putative polypeptides that were then aligned by MAFFT v7.0 (https://www.ebi.ac.uk/Tools/msa/mafft/). Phylogenetic analysis was computed using the maximum likelihood (ML) method with the Poisson correction distance of substitution rates of the Molecular Evolutionary Genetics Analysis (MEGA v7.0) program (Kumar et al., 2016). Neighbor joining (NJ) and minimum evolution (ME) trees were conducted both using the Poisson model with uniform rates and complete deletion. Bootstrap values were generated based on the 500 resampled data sets, using a 50% value as cut-off. All positions containing gaps and missing data were eliminated. The optimal tree from ML method was used as support for the other displayed NJ and ME trees, indicating the boostrap values in the branches of the ML tree.

The multiple sequence alignments for the putative α-galactosidases from *P. subrubescens* were performed using the structurally characterized α-galactosidase 4FNR from *Geobacillus stearothermophilus* as reference, and computed with MAFFT v7.0 and the ESPript v3.0 tools (http://espript.ibcp.fr/ESPript/ESPript/) (Sinitsyna et al., 2008) was used for alignment visualization.

The 3D homology models were accomplished with the SWISS-MODEL server (https://swissmodel.expasy.org/). The appropriate template was selected for specific protein modelling based on the best score interpreted by SWISS-MODEL. The quality and the stereochemistry of the final models was assessed and validated for different parameters using the combinatorial extension method (Prlić et al., 2010), ProSA (Wiederstein and Sippl, 2007), PROCHECK (Laskowski et al., 1996) and ProQ-Protein Quality Predictor (Wallner et al., 2003). Models were superimposed on templates and analyzed with UCSF Chimera (Pettersen et al., 2004).

In order to illustrate the possible substrate–protein interactions, the galactose-derived substrates that had the higher catalytic efficiencies were manually positioned into the active site by superimposition of the homology models with the structural oligomer found in the active site of various available crystal structures. In some uncharacterized AGLs, it was necessary to perform different simulations of the possible interactions of the galactose-ligands in the active site of the putative enzymes using the SWISS-DOCK (http://www.swissdock.ch/docking) program. The models with the galactose-derived substrate with minimum binding energy were selected and then filtered with respect to the orientation of the ligand in the active site according to the reports from crystal structures. In all cases, the ligand structures as well as the surrounding residues were exactly matching the crystal structure.

Theoretical isoelectric point (p*I*) and molecular weights (Mw) were calculated by ExPASy–ProtParam tool (https://web.expasy.org/compute_pi/).

2.2. Fungal culture conditions

Penicillium subrubescens FBCC1632/CBS132785 strain was cultivated in 50 mL of Minimal Medium (MM) (de Vries et al., 2004) containing 1% sugar beet pulp (SBP) as carbon source at 25 °C and 250 rpm, and a final concentration of 10^6 spores/mL. The mycelium was harvested after 24 h of incubation by vacuum filtration, dried between towels and frozen in liquid nitrogen. The mycelium samples were stored at −80 °C prior to RNA isolation.

2.3. cDNA cloning of P. subrubescens AGL encoding genes

Total RNA was extracted using TRIzol reagent (Invitrogen, Thermo Fischer Scientific, Carlsbad, CA) and purified by NucleoSpin RNA (Macherey-Nagel, Düren, Germany). Full-length cDNA was obtained using ThermoScript Reverse Transcriptase (Invitrogen). The mature AGL encoding genes, without the native signal peptide, were amplified by PCR from the cDNA. The PCR products from *aglA* (protein ID 10447), *aglC* (protein ID 10078) and *aglD* (protein ID 3476) were digested with the appropriate restriction enzymes (Promega, Madison, WI), and cloned in frame with *Saccharomyces cerevisiae* α-factor

secretion signal into the predigested plasmid pPICZαA (Invitrogen, Thermo Scientific, Carlsbad, CA). The PCR products of *aglB* (protein ID 2053), *aglE* (protein ID 4395), and *aglF* (protein ID 9225) were assembled in pPICZαA cloning vector using NEBuilder HiFi DNA Assembly Mix (New England Biolabs, Ipswich, MA) according to the manufacturer's protocol. The resulted plasmids were transformed and propagated into *Escherichia coli* DH5α competent cells (Invitrogen, Thermo Scientific, Carlsbad, CA) on low-salt Luria Bertani medium supplemented with 25 μg/mL Zeocin, and fully sequenced by Macrogen (Amsterdam, the Netherlands). The plasmids were linearized with *Pme*I or *Sac*I (Promega, Madison, WI), and transformed into *Pichia pastoris* X-33 cells by electroporation.

2.4. Production and purification of recombinant AGLs

P. pastoris transformants were selected on YPDS plates containing 1% yeast extract, 2% peptone, 2% glucose, 1 M sorbitol, 2% agar, and 100 μg/mL Zeocin. The transformants were grown in 3 × 400 mL BMGY medium (1% yeast extract, 2% peptone, 1.34% yeast nitrogen base with ammonium sulphate, 100 mM potassium phosphate, pH 6.0, 4×10^{-5}% biotin, 1% glycerol) at 30 °C for 24 h and 250 rpm. During the induction, the cells were resuspended in BMMY medium (100 mM potassium phosphate, pH 6.0, 1.34% yeast nitrogen base with ammonium sulphate, 1% casamino acid, 4×10^{-5} % biotin and 0.5% methanol) for 72 h at 22 °C, being supplemented with 0.5% (v/v) methanol every 24 h. Culture supernatants were harvested (8000 × *g*, 4 °C, 1 h), filtered (0.22 mm; Merck Millipore, Darmstadt, Germany), and concentrated though a Vivaflow 200 membrane of 10 kDa molecular weight cutoff (Sartorius AG, Goettingen, Germany). The crude extract was loaded onto a HisTrap FF 1 mL column equilibrated with 20 mM HEPES, 0.4 M NaCl, 20 mM imidazole, pH 7.5. All chromatographic steps were carried out with columns coupled to an ÄKTA FPLC device (GE Life Sciences, Uppsala, Sweden). Proteins were eluted using a linear gradient of 22–400 mM imidazole in the buffer mentioned above at a flow rate 1.0 mL/min. Fractions containing enzyme were pooled, concentrated and buffer-exchanged to 20 mM HEPES, pH 7.0, in 10 kDa cut-off ultrafiltration units Amicon (Millipore). All purification steps were performed at 4 °C.

2.5. Physical properties of AGLs

The molecular mass of purified enzymes was estimated by sodium dodecyl sulfate–polyacrylamide gel electrophoresis (12% w/v, SDS-PAGE) using Mini-PROTEAN Tetra Cell (Bio-Rad, Hercules, CA) and the standard marker, PageRuler™ Plus Prestained Protein ladder (Thermo Fisher Scientific) with Coomassie Brilliant Blue staining (Bio-Rad). Deglycosylation was performed by treating the native enzymes with endoglycosidase H (New England Biolabs, MA) according to the manufacturer instructions. The protein concentration was determined by a Bradford assay with bovine serum albumin (Pierce, Thermo Scientific) as standard.

2.6. Enzyme activity assays and enzyme stability

For assessment of α-galactosidase activity, *p*-nitrophenyl-α-D-galactopyranoside (*p*NPαGal) (Sigma Aldrich) was used as a substrate. The activities were assayed in a total volume of 100 μL reaction mixtures containing 10 μL of 2 mM *p*NPαGal in 50 mM sodium acetate buffer, pH 5.0, and 0.2–0.3 nM purified enzymes at 30 °C. The release of *p*-nitrophenol was spectrophotometrically quantified by following the absorbance at 405 nm in a microtiter plate reader (FLUOstar OPTIMA, BMG LabTech, Germany) for 30 min with a 2 min interval. One unit of enzymatic activity was defined as the amount of protein required to release one μmol of the corresponding product per minute, under the assay condition used.

The effect of pH on the recombinant α-galactosidases was determined over different pH range of 2.0–12.0 using 40 mM Britton-Robinson buffer (adjusted to the required pH) at 30 °C, under the conditions described above, excepting that the reaction was stopped after 30 min with 100 μL 0.25 M Na_2CO_3. The pH stability was analyzed by incubating the enzymes in the same buffer system in the range from pH 2.0 to pH 12.0 for 1 h and then determining their residual activities by the standard assay in 50 mM sodium acetate, pH 5.0, at 30 °C. The effect of temperature on the recombinant α-galactosidases was determined over the temperature range of 10–90 °C at their optimum pH values, essentially as above. Thermostability was investigated by measuring the enzyme activity remaining after incubation for 1 h at 10–90 °C.

2.7. Enzyme kinetics

Kinetic parameters of the Michaelis–Menten constant (K_m), maximum enzyme velocity (V_{max}), turnover number (k_{cat}), and the catalytic efficiency (k_{cat}/K_m) were measured by determining the enzyme initial activities over defined concentration ranges of galactose-derived substrates. The substrate concentrations analyzed were 0.25–7.0 mM for *p*NPαGal, and 2.0–10.0 mM for melibiose, raffinose, and stachyose. The *p*NPαGal enzyme initial activities were determined during 30 min using the same experimental and assay conditions described above for each enzyme. Initial rates of hydrolysis of galacto-oligosaccharides were measured in 40 mM Britton-Robinson buffer at the optimum pH and temperature of each enzyme. Aliquots of 100 μL were removed at 10, 20, 30, 40, 50, and 60 min and mixed with 400 μL of 100 mM NaOH to stop the reaction. Galactose released from melibiose, raffinose and stachyose was quantified with high-performance anion-exchange chromatography with pulsed amperometric detection (HPAEC-PAD) on a Dionex ICS-5000+ chromatography system (Thermo Fisher Scientific, Sunnyvale, CA). The chromatograms were processed on a Chromelen system (Thermo Fisher Scientific). Kinetic parameters were estimated by fitting the Michaelis–Menten equation to initial rates with GraphPad Prism v.5.0 (GraphPad Software Inc., La Jolla, CA).

2.8. Activity towards galactomannan-based polysaccharides

Hydrolysis of galactomannan-based lignocellulosic substrates was measured using 3 μg/mL of recombinant enzyme or with the addition of 3 U of a commercial endomannanase from *Aspergillus niger* (Megazyme, Wicklow, Ireland), and 1% of guar gum (Sigma-Aldrich), carob galactomannan (Megazyme) or locust bean gum (Sigma-Aldrich), in 50 mM sodium acetate buffer (pH 4.0). The samples were incubated for 24 h at 30 °C and 100 rpm. Saccharification reactions were stopped by incubation at 95 °C for 15 min after which the samples were centrifuged (10 min, 4 °C, 13 500 × *g*) and the supernatant was diluted 10-fold in milliQ water prior the analysis. The released galactose was quantified using HPAEC-PAD (Dionex ISC-5000+ system, Thermo Fisher Scientific, Sunnyvale, CA), equipped with a CarboPac PA1 (250 mm × 4 mm i.d.) column (Thermo Fisher Scientific). The column was pre-equilibrated with 18 mM NaOH followed by a multi-step gradient: 0–20 min: 18 mM NaOH, 20–30 min: 0–40 mM NaOH and 0–400 mM sodium acetate, 30–35 min: 40–100 mM NaOH and 400 mM to 1 M sodium acetate, 35–40 min: 100 mM NaOH and 1 M to 0 M sodium acetate followed by re-equilibration of 18 mM NaOH for 10 min (20 °C; flow rate: 0.30 mL/min). 5–250 microM D-galactose (Sigma-Aldrich) was used as standards for quantification. The data obtained are the results of two independent biological replicates and for each replicate three technical replicates were assayed. The galactose released was calculated as a percentage of the highest hydrolysis reached for each treatment, which was set to 100%.

To investigate the interaction between each recombinant enzyme and the commercial endomannanase, the degree of synergy (DS) was calculated as the ratio between the concentration of galactose released by the enzyme mixture and the theoretical sum of galactose released by

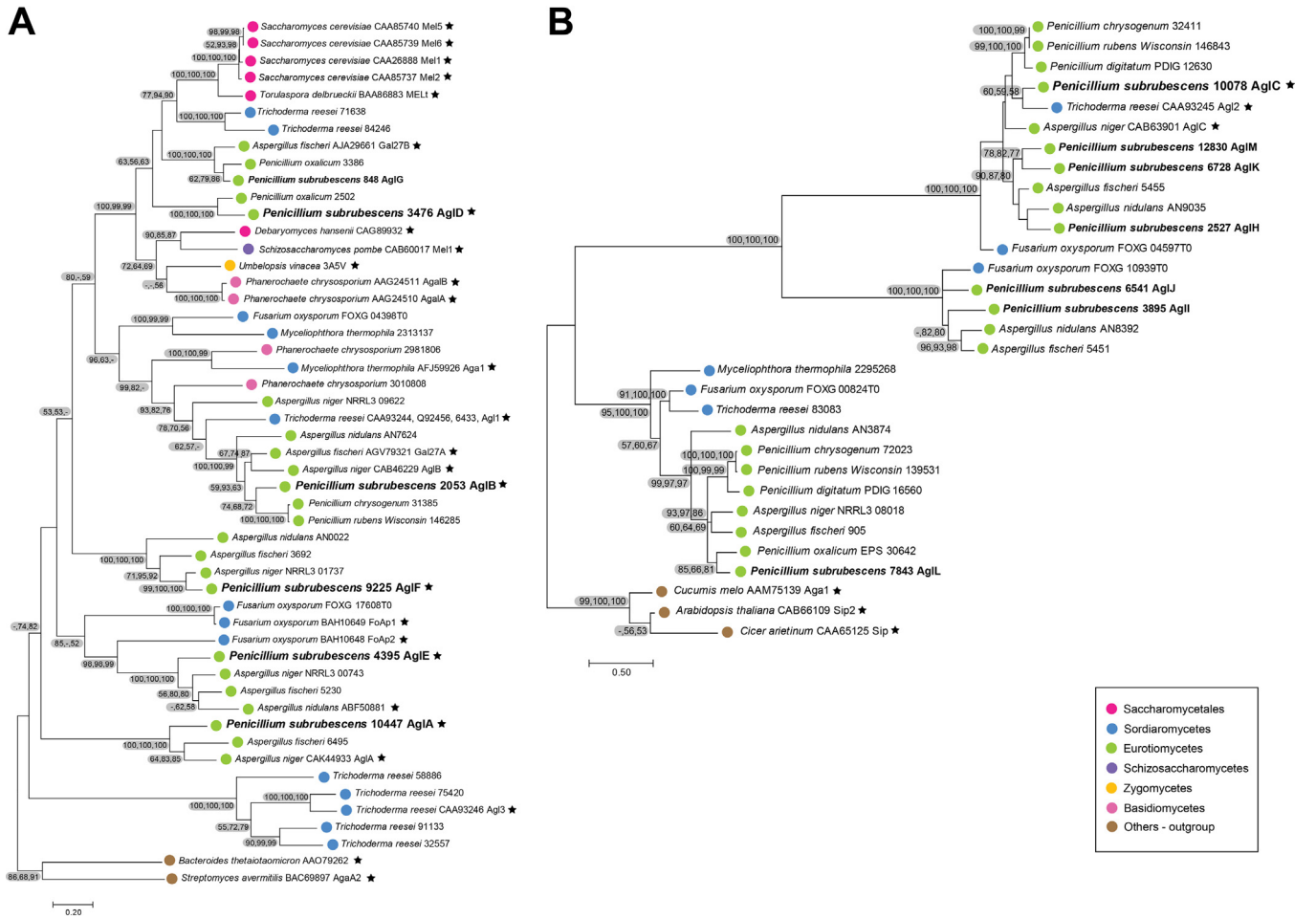

Fig. 1. Analysis of phylogenetic relationships among the (putative) fungal α-galactosidases from *P. subrubescens* and selected fungal species from GH27 (A) and GH36 (B). The phylogram was inferred using the Maximum likelihood (ML) method and the optimal tree is shown. Values over 50% bootstrap support (500 replicates) are shown next to the branches in grey ovals using ML (first position), neighbour-joining (NJ, in second position) and minimal evolution (ME, in third position) tree values from the same dataset. AGLs from *Bacteroides thetaiotaomicron*, *Streptomyces avermitilis*, *Cucumis melo*, *Arabidopsis thaliana* and *Cicer arietinum* were used as an outgroup. The bar indicates the number of substitutions per site. The putative *P. subrubescens* α-galactosidases were highlighted and the characterized proteins were denoted with a black star.

the individual enzymes.

3. Results and discussion

3.1. Phylogenetic analysis reveals high diversity of secreted α-galactosidases in Penicillium species

Compared to other members of the same phylum, *P. subrubescens* contains a much larger number of selected plant biomass degrading enzymes, including putative AGLs (de Vries et al., 2017; Peng et al., 2017). To gain deeper insight into the classification status of putative α-galactosidases from *P. subrubescens*, two phylogenetic trees of GH27 and GH36 families were generated based on 51 and 31 amino acid sequences, respectively, including characterized enzymes from fungal origin (Fig. 1). The GH27 and GH36 families are structurally and phylogenetically related and form clan GH-D, which included most of the experimentally identified α-galactosidases (Naumoff, 2011). The *in silico* study revealed that *P. subrubescens* has six members from GH27, of which five contained a secretory signal peptides in their sequences. In contrast, seven putative α-galactosidases were found in GH36 with only one protein containing a secretory signal peptide. This high number of extracellular GH27 proteins compared to those of GH36, has been observed previously in other fungi, where most extracellularly active α-galactosidases belong to GH27, while a small portion belong to GH36 (Ademark et al., 2001b; Bauer et al., 2006; Morales-Quintana et al., 2017; Nakai et al., 2010). This has been suggested to have evolutionary origin, being caused horizontal transfer of GH27 AGLs from eukaryotes to bacteria, while the opposite may have occurred for GH36 AGLs (Naumoff, 2004).

The phylogenetic analysis showed that AglA, AglB, AglE and AglF from *P. subrubescens* were clustered together with other GH27 proteins from eurotiomycetes, such as *Aspergillus niger*, *Aspergillus fischeri*, *Aspergillus nidulans*, *Penicillium chrysogenum, Penicillium rubens* and *Penicillium digitatum* (Fig. 1A). However, the vast majority of these proteins has not been characterized at present. Similarly, *P. subrubescens* AglD and AglG were part of a cluster together with proteins from eurotiomycetes, saccharomycetales and sordariomycetes species, such as *S. cerevisiae*, *Toluraspora delbrueckii* and *T. reesei* (Fig. 1A).

Phylogenetically, AglC had high identity to characterized GH36 α-galactosidases of *A. niger* (AglC) and *T. reesei* (Agl2), as well as uncharacterized proteins from other *Penicillium* species (Fig. 1B). Therefore this gene was referred to as *aglC* as well, to avoid confusion when comparing it to the *A. niger* genes. Moreover, the other six putative GH36 proteins (without signal peptide) from *P. subrubescens*, were clustered with other eurotiomycetes and with sordariomycetes sequences, but not directly with characterized proteins (Fig. 1B), likely due to the fact that they are intracellular enzymes.

Interestingly, the biochemically characterized enzymes from this

Table 1
Properties and specific activities towards *p*NP-α-D-galactopyranoside of recombinant *P. subrubescens* α-galactosidases produced by *P. pastoris*.

Protein ID at JGI	Enzyme code	CAZy family	Mass (kDa)			Specific activity U/mg*
			calculated	before Endo H	after Endo H	
10,447	AglA	GH27	59.1	63	59	62
2053	AglB	GH27	48.8	65	55	279
3476	AglD	GH27	55.3	70	56	256
4395	AglE	GH27	71.6	85	72	30
9225	AglF	GH27	45.5	60	46	100
10,078	AglC	GH36	82.7	90	83	17,475

* One unit of α-galactosidase activity is defined as the amount of protein required to release one μmol of the corresponding product per minute.

study are relatively close to α-galactosidases from *Aspergillus* species (Ademark et al., 2001a; de Vries et al., 1999). This close distance between those enzymes may reflect a similar mode of action of those enzymes against galacto-derived substrates.

3.2. P. pastoris transformants secreted high levels of active AGLs

The mature polypeptide of the six candidate AGLs from *P. subrubescens* that contained a secretion signal from GH27 (AglA, AglB, AglD, AglE, and AglF) and GH36 (AglC), were produced as C-terminal His-tag fusion proteins in *P. pastoris*. The recombinant proteins were purified from *P. pastoris* culture supernatants and the specific activities were estimated using *p*NPαGal as substrate. High specific activities were obtained (up to 17,475 U/mg, Table 1) compared to native α-galactosidases secreted by *Penicillium canescens* (1255 U/mg) (Sinitsyna et al., 2008), *Penicillium simplicissimum* (192 U/mg) (Luonteri et al., 1998b) or *A. niger* (1080 U/mg) (Ademark et al., 2001b), and recombinant *Penicillium purpurogenum* (986 U/mg) (Morales-Quintana et al., 2017), *Penicillium janczewskii* (667 U/mg) (Chen et al., 2012) or *A. niger* (1299 U/mL) (Zheng et al., 2016) α-galactosidases produced in *P. pastoris*.

3.3. N-glycosylation revealed extensive glycosylation of rAGLs produced in P. pastoris

The purified recombinant proteins migrated on SDS-PAGE as a single band with an increased molecular mass over a range of 4–15 kDa (Fig. 2A/Table 1), suggesting heterogeneous glycosylation. This was confirmed by treatment with endoglycosidase H. The treated proteins showed a molecular size similar to their predicted mass as shown in Fig. 2A and Table 1. A high level of glycosylation is common in secreted proteins produced by *P. pastoris* (Kamal et al., 2018; Morales-Quintana et al., 2017).

3.4. rAGLs show a broad pH and temperature stability

AglA, AglB, AglC, AglE and AglF share the same pH optimum on *p*NPαGal activity at pH 4, while AglD showed a pH optimum at pH 5.0 (Fig. 2B). AglA and AglD were stable at pH 3.0–7.0, whereas AglB and AglE were stable at pH 3.0–6.0, and AglC and AglF were stable at pH 2.0–6.0 and pH 2.0–8.0 respectively, with more than 80% residual activity (Fig. 2B). This result suggested that, in this pH range, there was no significant change in the overall structure in most recombinant enzymes.

AglA, AglB, AglD, and AglE showed maximum activity at 40 °C, while AglC and AglF displayed maximum activity at 50 °C (Fig. 2C). These properties are within range of other fungal α-galactosidases with reported activity optima at pH 4.0–5.0 and 40–50 °C (Kurakake et al., 2011; Nakai et al., 2010; Sinitsyna et al., 2008; Zeilinger et al., 1993). In general, the enzymes showed a broad thermostability, being a favorable property for the increased reaction rates at high temperatures and lower risk of contamination in industrial applications (Aulitto et al., 2019). AglB, AglD, and AglE retained more than 80% activity after 1 h incubation up to 40 °C, whereas AglA and AglC maintained 80% activity up to 50 °C, and AglF up to 60 °C (Fig. 2C). AglF was highly stable over a much broader pH and temperature range, making it one of the most attractive candidates for industrial applications.

3.5. rAGLs hydrolyze a broad range of natural galacto-oligosaccharides with high catalytic efficiencies

The substrate specificities of rAGLs were investigated towards the synthetic substrate *p*NPαGal, and the galacto-oligosaccharides: melibiose, raffinose and stachyose (Table 2). AglB and AglD had the highest affinity (K_m = 0.13 mM) and catalytic efficiency (k_{cat}/K_m = 4164 and 4866 $mM^{-1}s^{-1}$, respectively) for *p*NPαGal (Table 2). Nevertheless, all enzymes showed higher affinity for this synthetic substrate than for the galacto-oligosaccharides. This is a common feature for most fungal α-galactosidases, which may be due to the simple molecular structure of *p*NPαGal (Morales-Quintana et al., 2017; Nakai et al., 2010; Sinitsyna et al., 2008).

For the galacto-oligosaccharide substrates tested, AglB, AglC and AglF exhibited the highest affinity for the tetrasaccharide stachyose (Table 2). The catalytic efficiency showed that stachyose was used most efficiently by AglB, followed by AglC, and AglF (Table 2), suggesting that these enzymes are more efficient when the chain length of the oligosaccharide increases. Likewise, recombinant AglB, AglC, AglD, and AglF enzymes showed the lowest K_m value and the highest catalytic efficiencies towards the trisaccharide raffinose (Table 2). These results strongly suggest that the hydrolysis of raffinose and product formation occurred faster by these enzymes, than for other published AGLs (Liao et al., 2016; Nakai et al., 2010; Sinitsyna et al., 2008). In addition, AglC and AglF showed the highest affinity and catalytic efficiencies for the disaccharide melibiose, whereas the opposite behavior was observed for AglD. AglA showed a lower affinity towards the three oligosaccharides tested (Table 2), while AglE did not show any detectable hydrolytic activity towards the galacto-oligosaccharides containing α-(1,6)-linked galactose, although it was active against synthetic *p*NPαGal. The affinity of AglE towards *p*NPαGal, but not against galacto-oligosaccharides is quite comparable to that of *Fusarium oxysporum* α-galactosidase Fo/AP2 (Sakamoto et al., 2010), suggesting that the enzyme activity is affected by the structure of substrates.

3.6. 3.6 Hydrolysis of galactomannan-based lignocellulosic substrates is enhanced by synergistic action of rAGLs and a commercial mannanase

Effective enzymatic hydrolysis of the galacto(gluco)-mannan present in hemicellulosic substrates to fermentable sugars or biochemicals, requires a combination of various glycoside hydrolases whose combined action could be more efficient than the sum of the individual enzymes. In this study, the rAGLs were evaluated to determinate their catalytic potential during the conversion of galactomannan-based lignocellulosic substrates to release galactose residues, as well as their synergistic interactions with a commercial GH27 endomannanase from *A. niger*. The hydrolysis of guar gum, carob galactomannan, and locust bean gum was set up at 30 °C and pH 4.0 to ensure the optimal activity and stability of the endomannanase.

Under the conditions tested, the highest galactose release on guar gum (58%) was observed for AglB (Fig. 3A). When guar gum was depolymerized with AglB in the presence of endomannanase, a significant increase in galactose release was observed (Fig. 3). However, the degree of synergy (DS) between AglB and endomannanase was about 1.7, indicating that the observed improvement in guar gum hydrolysis was more a product of AglB acting independently (Table 3). AglA and AglE showed very low hydrolysis of guar gum, and no significant

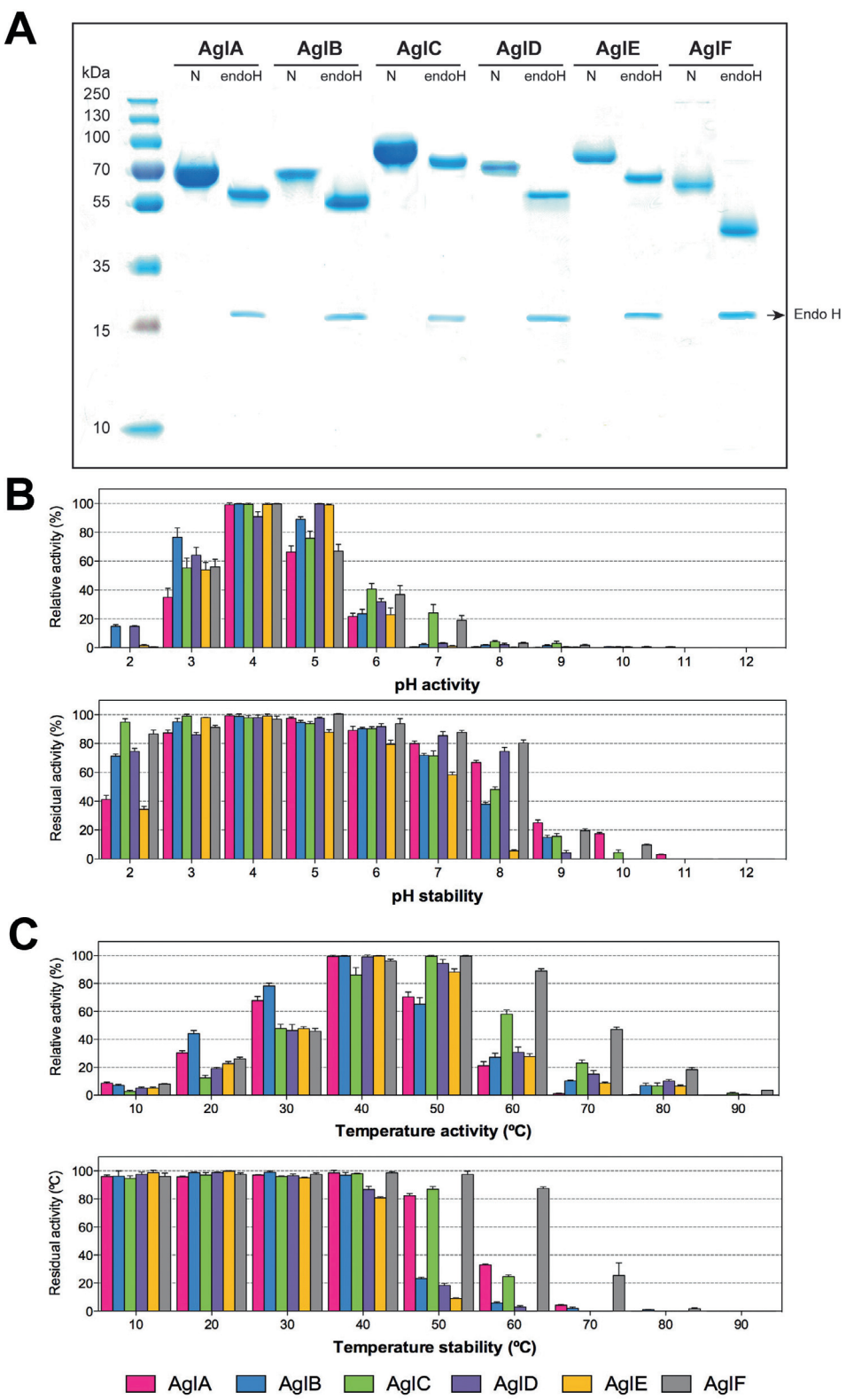

Fig. 2. Molecular mass analyses and enzymatic properties of the recombinant α-galactosidases produced in *P. pastoris*. SDS-PAGE analysis (A) of the purified recombinant α-galactosidases without (N) and with endoglycosidase H treatment. Effect of pH (B) and temperature (C) on the activity and stability of recombinant α-galactosidases using *p*NPαGal as substrate. The pH and temperature-dependence for activity was evaluated at 30 °C in 40 mM Britton-Robinson buffer, pH 2.0–12.0, or in 50 mM sodium acetate, pH 5.0, at 10–90 °C, respectively. The pH and temperature stability was deduced from the residual activity after 1 h of incubation. All assays were carried out in triplicate.

contribution by the addition of the endomannanase in galactose release was observed (Fig. 3A). This result can be only explained by the low or undetectable affinity of AglA and AglE towards galacto-oligosaccharides as previously mentioned (Table 2).

Although a lower galactose release by AglC and AglF was observed under the same conditions (about 3%), a DS about 8 and 3 was obtained when the endomannnase was supplemented (Fig. 3A, Table 3). There are several possible explanations for the strong synergistic interaction observed between the enzymes despite their low individual performance. Probably the endomannanase increased the proportion of substrate available for the α-galactosidases by releasing small galactose-containing oligosaccharides that are preferable substrates for AglC and AglF (see Section 3.5). A previous study (Wang et al., 2014) also found that only the simultaneous addition of mannanases and α-

Table 2
Kinetic parameters for hydrolysis of *p*NPαGal and galacto-oligosaccharides catalyzed by recombinant AGLs from *Penicillium subrubescens*. Parameters were calculated from the initial velocities of *p*NP released from *p*NPαGal and galactose from melibiose, raffinose and stachyose at different substrate concentrations. Gal = galactose, Glc = glucose, Frc = fructose. ND = not detected.

Enzyme	CAZy family	*p*NPαGal			melibiose (Gal-α(1 → 6)-Glc)			raffinose (Gal-α(1 → 6)-Glc-α(1 → 2β)-Frc)			stachyose (Gal-α(1 → 6)-Gal-α(1 → 6)-Glc-α(1 ↔ 2β)-Frc)		
		K_m (mM)	k_{cat}(s^{-1})	k_{cat}/K_m (mM^{-1} s^{-1})	K_m (mM)	k_{cat} (s^{-1})	k_{cat}/K_m (mM^{-1} s^{-1})	K_m (mM)	k_{cat} (s^{-1})	k_{cat}/K_m (mM^{-1} s^{-1})	K_m (mM)	k_{cat} (s^{-1})	k_{cat}/K_m (mM^{-1} s^{-1})
AglA	GH27	0.69	312.5	456	8.47	34.2	4	8.71	62.6	7	7.08	45.4	6
AglB	GH27	0.14	573.9	4165	1.36	94.5	70	0.60	871.1	1452	0.21	747.6	3484
AglD	GH27	0.14	680.4	4867	37.70	18.6	0.5	0.94	138.9	147	7.94	184.3	23
AglE	GH27	0.73	588.6	803	ND	ND	ND	ND	ND	ND	ND	ND	ND
AglF	GH27	0.28	375.7	1347	0.27	684.2	2553	0.85	402.6	472	0.52	596.4	1149
AglC	GH36	0.26	1050.4	4114	0.60	828.2	1393	0.67	673.5	1008	0.56	744.3	1327

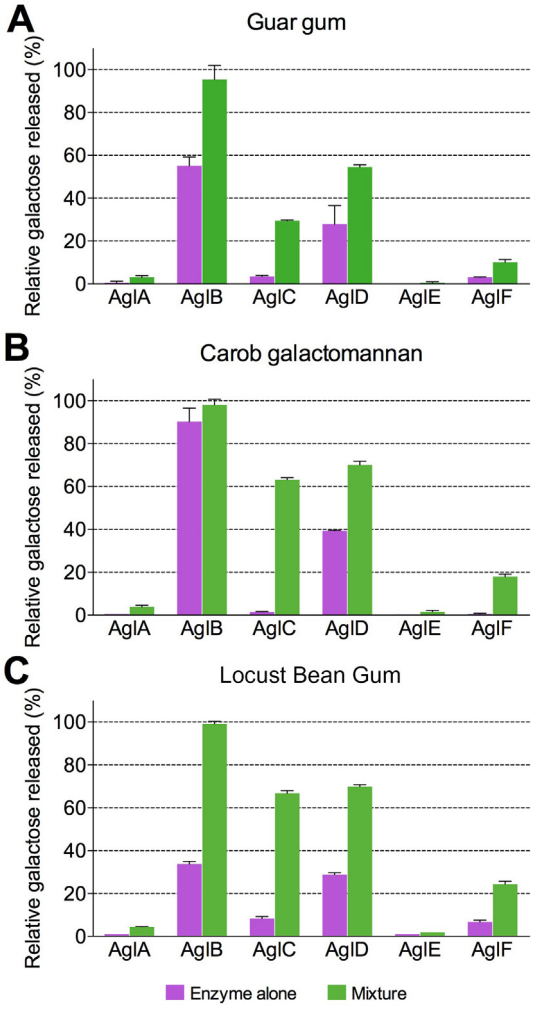

Fig. 3. Galactomannan-based lignocellulosic substrate hydrolysis by recombinant α-galactosidases. (A) Guar gum, (B) carob galactomannan, and (C) locust bean gum substrates (1%) were incubated with 3 µg/mL of recombinant enzyme or with the addition of 3 U of a commercial endomannnanase from *A. niger*. Hydrolysis was performed at 30 °C for 24 h. The relative galactose released was calculated as a percentage of the highest hydrolysis reached for each treatment, which was set to 100%. Values are represented as mean values ± SD (n = 2).

galactosidases enhanced guar gum hydrolysis, reaching the highest synergistic interaction in comparison with the almost undetectable activity of the enzymes alone.

As shown in Fig. 3B, carob galactomannan conversion followed a similar pattern to guar gum conversion: addition of endomannanase improved the overall conversion when compared to the α-galactosidases alone. Overall, hydrolysis of carob galactomannan was higher than that of guar gum. These differences can be explained by the higher extent of galactose substitutions on the mannan backbone of guar gum, which makes the debranching of the substrate by the α-galactosidases more critical (Aulitto et al., 2018; Song et al., 2018). Notably, AglB alone achieved about 90% of relative galactose release, while the combination with endomannanase produced the highest sugar release (about 100%), but the higher release of galactose did not correspond with a high DS value, 1.08 (Table 3). From this data, it was evident that AglB had very strong capacities of degrading galactomannan alone, while in contrast, AglC was strongly enhanced by the presence of endomannanse, reaching a DS of 27 (Table 3), which confirms the results described in Section 3.5. Usually, the members of GH36 show low affinity towards polymers, attributing it mainly to the larger size of the enzymes that restricts their ability to access the galactose residues on the polymers (Mi et al., 2007).

As expected, the hydrolysis pattern of the recombinant α-galactosidases on locust bean gum was similar to that obtained on guar gum and carob galactomannan. Hydrolysis of locust bean gum by AglB and AglD, operating independently, displayed a similar release of galactose, while the synergy degree of both enzymes with endomannnanase reached up to 2 (Fig. 3C, Table 3). Thus, it is reasonable to suggest that AglB has better performance on hydrolyzing guar gum and carob galactomannan compared to locust bean gum, since the galactose content of carob galactomannan and locust bean gum is almost the same (Aulitto et al., 2018). In contrast, the increased release of galactose by the individual enzymes AglC and AglF from locust bean gum could indicate that these fungal α-galactosidases can degrade parts of locust bean gum, which are inaccessible for the other rAGLs (Fig. 3C, Table 3). In this regard, different studies have shown that the degree of synergy between galactomannanolytic enzymes does not depend solely on their properties, but also on the properties of the substrate to be hydrolyzed

Table 3
Synergistic action between commercial endomannanase from *A. niger* (Anman) and recombinant α-galactosidases from *P. subrubescens* on hydrolysis of galactomannan-based lignocellulosic substrates. The degree of synergy (DS) was calculated as the ratio between the concentration of galactose released by the enzyme mixture and the theoretical sum of galactose released by the individual enzymes.

Substrate	Degree of synergy (DS)					
	AglA	AglB	AglC	AglD	AglE	AglF
Guar gum	4.47	1.73	8.05	1.95	1.34	3.18
Carob galactomannan	2.89	1.08	27.59	1.74	1.58	14.64
Locust bean	1.97	2.84	7.03	2.34	0.86	3.10

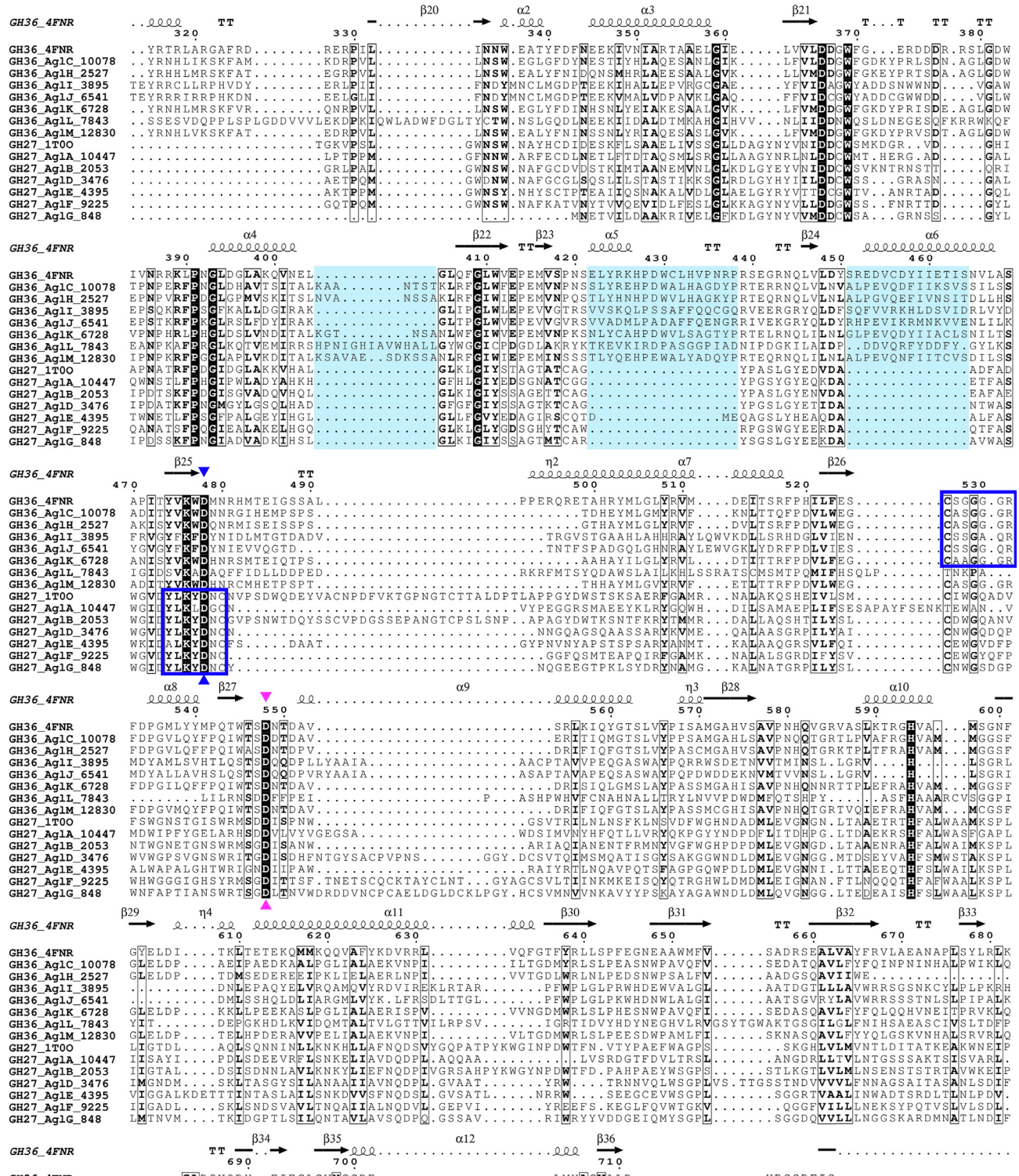

(caption on next page)

Fig. 4. Amino acid sequence alignment of characterized and uncharacterized GH27 and GH36 α-galactosidases from *P. subrubescens*. The secondary structure assignment refers to 4FNR from *Geobacillus stearothermophilus* GH36 structural model. The GH27 α-galactosidase 1T0O amino acid sequence from *T. reesei* was included in this analysis. The α-helices are shown as spirals labelled (α), β-strands are shown as arrows labelled (β) and β-turns are labelled (TT). The black squares indicate sequence similarity, and identical residues are shown in black background. The insertions are highlighted with a blue box. Blue triangles indicate putative nucleophile residues and the magenta triangles indicate putative acid/base catalytic residues. The dark blue squares indicate the presence of sequence motifs. (For interpretation of the references to color in this figure legend, the reader is referred to the web version of this article.)

(Aulitto et al., 2018; Malgas et al., 2015; Wang et al., 2014).

3.7. 3.7 Differences in the catalytic domain of recombinant α-galactosidases affect their productive binding for galactose-derived substrates

The sequence alignment revealed conserved amino acids among GH27 and GH36 members of *P. subrubescens* (Fig. 4), showing in general highly conserved sequences at the catalytic domain, but to a lesser extent in the C-terminal domain. Indeed, the position and conservation of these residues correlate with the consensus motifs YLKYDNC and CXXGXXR (Fig. 4), which are involved in galactose recognition and are located within the N-terminal region of GH27, or in the central region of GH36 (Fredslund et al., 2011; Hart et al., 2000). However, it was not possible to identify any consensus motif in the amino acid sequence of AglE (Fig. 4). The absence of such a conserved sequence could explain the lack of productive bining of this enzyme towards the galacto-oligosaccharides and the galactomannan-based lignocellulosic substrates. Moreover, GH27 and GH36 α-galactosidases from *P. subrubescens* share the presence of two fully conserved aspartic acid residues involved in the nucleophile and acid–base catalytic mechanism (Fig. 4), as previously reported in other α-galactosidases (Fernández-Leiro et al., 2010; Fredslund et al., 2011; Golubev et al., 2004).

A comparison of the active site of the characterized rAGLs was performed using available crystal structures and homology models to explore the substrate binding sites between galacto-derived substrates and the catalytic pocket. The enzymes characterized here show high amino acid sequence identity to other GH27 and GH36 AGLs. Overall, AglA has highest sequence identity with 6F4C *Nicotiana benthamiana* α-galactosidase (36%), AglB with 1T0O *T. reesei* (60%), AglC with 4FNR *G. stearothermophilus* (43%), AglD with 3LRL *S. cerevisiae* (49%), AglE with 1UAS *Oryza sativa* (40%), and AglF with 3A5V *Mortierella vinacea* α-galactosidase (37%).

Based on homology with an α-galactosidase of *Nicotania benthamiana* (PDB ID: 6F4C) from GH27, whose catalytic residues have been identified, it is highly probable that the catalytic residues of AglA are Asp^{131} and Asp^{201}, whereas in the active site other amino acids appear involved in substrate recognition (Table 4, Fig. 5A) (Kytidou et al., 2018). Nonetheless, a short insertion of seven residues (PAYFSEN) located in the position β27 of the vicinity of the catalytic site was observed in the AglA structure (Fig. 4). Apparently, the insertions surrounding the catalytic center may be involved in rearrangements of the spatial position of catalytic domain, which is related to changes in the specificity towards long substrates (Fernández-Leiro et al., 2010). Similar considerations may be applied to explain the low specificity of the enzyme towards galacto-oligosaccharides, as well as long galactomannan branches.

The comparison of structures of AglB and an α-galactosidase from *T. reesei* (PDB ID: 1T0O) point out interesting features in the models (Fig. 5B). The first galactose unit of the substrate stachyose in AglB is located between two aspartic acids (Asp^{133} and Asp^{225}) that act as the catalytic residues, whereas it is hydrogen-bonded to different residues, as shown in Fig. 5B and Table 4. Notably, adjacent to the catalytic pocket, one water-mediated hydrogen bond was formed by the hydroxyl group of Tyr^{97} with the galactose oligomer, which is absent in the homologous 1T0O crystal structure (Golubev et al., 2004). The importance of tyrosine for substrate-binding was corroborated by replacement of alanine by a tyrosine in the catalytic site of *S. cerevisiae* α-galactosidase GH27 (Fernández-Leiro et al., 2010). This replacement demonstrated that the presence of tyrosine may be crucial to the stability and affinity for the oligomer. Consequently, the cluster made up of residues Trp^{18}, Trp^{204}, Cys^{105}, Cys^{135}, Met^{257}, Arg^{221} and Cys^{202} probably creates a long and wide cavity that can readily accommodate long substrate chains (Fig. 5B). This likely contributes to direct interactions and differentiated degradation pattern of galactomannans, findings that are consistent with the biochemical data presented here.

The homology modelling analysis revealed that the main features observed at the galactose-binding pocket in the AglD-raffinose complex are consistent with that described previously for an α-galactosidase from *S. cerevisiae* (PDB ID: 3LRL) (Fernández-Leiro et al., 2010). The model of AglD appears to have a deep and narrow pocket evolved to accommodate the galactopyranosyl residue of raffinose that interacts with the residues Asp^{128} and Asp^{188} (Table 4, Fig. 5C). A closer analysis of the two models reveals that the principal difference between these structures is the presence of Tyr^{208} and Gly^{224} residues in the binding pocket of AglD, while Phe^{235} and Gln^{251} are superposed on the same position in 3RLR (Fig. 5C). In this respect, it is relevant to mention that previous work on 3RLR (Fernández-Leiro et al., 2010) has shown that an insertion found at Phe^{235} stabilized the substrates in the active site, whereas the Gln^{251} residue was proven to be essential for activity. According to Fernández-Leiro et al. (Fernández-Leiro et al., 2010), a change of glutamine to alanine can significantly decrease the affinity towards melibiose and raffinose, or make 3RLR more active against *p*NPαGal. Remarkably, Tyr^{208} is located close to the catalytic pocket and is able to stabilize the fructose moiety of raffinose by direct interaction through hydrogen bond, whereas the change of Gln^{251} to Gly^{224} makes the catalytic pocket more open and accessible (Fig. 5C). These modifications could be a major factor to explain the broad affinity of AglD to galactomannan-derived substrates.

Examination of models for AglE and an α-galactosidase from *O. sativa* (PDB ID: 1UAS) showed significant differences in the architecture of AglE (Fig. 5D, Table 4). As can be seen in Fig. 5D, residues Asp^{138} and Asp^{205} in the AglE active site are aligned surrounding the docked *p*NPαGal molecule. Nevertheless, the modelling revealed the presence of Tyr^{22} and Cys^{58} in the active site of AglE, which vary in the structure of 1UAS by the residues Trp^{16} and Asp^{52} (Fig. 5D). In this respect, Fujimoto et al. (Fujimoto et al., 2003) deduced that Trp^{16} and Asp^{52} contribute partially in the catalysis of galacto-oligosaccharides and are involved in important hydrophobic interactions with the ligand. This observation suggests that the presence of Tyr^{22} and Cys^{58} affects the conformation of AglE provoking a narrower and more restrained catalytic pocket (Fig. 5D), and perhaps obstructing the accommodation of long galactomannan branches. Altogether, the absence of consensus motif YLKYDNC combined with significant differences in the space available in the catalytic pocket provide a possible explanation for the low affinity of the AglE towards galacto-oligosaccharides and complex polysaccharides, although the kinetic analysis clearly demonstrated that AglE is able to hydrolyze *p*NPαGal.

The superposition of the models revealed that the spatial position of the catalytic site of AglF coincides well with the model from *Mortierella vinacea* α-galactosidase (PDB ID: 3A5V). Like other α-galactosidases of GH27 reported previously, four conserved residues in AglF (Asp^{128}, Asp^{186}, Cys^{100} and Cys^{130}) are localized in the catalytic domain, and six residues correspond to the substrate binding site of the complex with melibiose (Table 4). However, the model of AglF exhibits a narrower active site cleft (Fig. 5E) that probably limits its affinity towards long galacto-polymers. In contrast, the docking analysis of AglG

Table 4
Comparative overview of the putative residues involved in substrate binding in the structurally characterized α-galactosidases from PDB and the homology modelled α-galactosidases from *P. subrubescens*.

Protein name	Model ID	Structure ID	Model substrate	Catalytic residues		Binding residues	
				Model	Structure	Model	Structure
GH27							
AglA	10,447	6F4C	stachyose	D131, D201	D267, D236	W18, E22, D53, D54, Y95, C103, C133, V204, F239	W67, D102, D103, Y144, C152, C183, R232
AglB	2053	1T0O	stachyose	D133, D225	D132, D226	W18, D53, D54, K131, Y97, C105, C135, C202, W204, R221	W19, D54, D55, K130, C104, W205, R222
AglD	3476	3LRL	raffinose	D128, D188	D149, D209	D51, D52, Y92, K126, C100, C165, W167, R184, Y208, G224	D72, D73, Y113, C121, A122, K147, R205, F235, Q251
AglE	4395	1UAS	pNPαGal	D138, D205	D130, D185	Y22, D57, C58, Y99, K136, C182, W184, R201, M237	W16, Y93, C101, S102, K128, W164, R181, D216
AglF	9225	3A5V	melibiose	D128, D186	D149, D209	D50, D51, Y92, A101, K126, C100, C130, C163, W165, G208	W37, D72, D73, Y113, A122, C121, C152, C186, W188, R205, G234
AglG	848	3LRL	melibiose	D106, D166	D149, D209	C78, A79, K104, C143, W145, R162, Y193, S209, K210	D72, D73, C121, A122, K147, C186, W188, G234, F235
GH36							
AglC	10,078	4FNR	stachyose	D500, D562	D478, D548	W78, D378, D379, R465, K498, W433, N502, S542, G543, Q595	D53, A55, R65, W199, Y340, D366, D367, W411, K476, C526, G528, G529
AglH	2527	4FNR	raffinose	D482, D544	D478, D548	D360, D361, W330, W415, R447, K480, C522, S524, G525, N484	D53, A55, R65, W199, Y340, D366, D367, W411, K476, C526, G528, G529
AglK	6728	4FNP	pNPαGal	D183, D243	D478, D548	R184, S185, L145, R146, A222, A223, G226, R227	D53, R65, Y340, D366, D367, W411, K476, C526, G528, G529
AglM	12,830	4FNS	raffinose	D508, D548	D478, D548	W351, D381, D382, F356, D394, W441, R473, K506, N510, C548, S550, G551	D53, A55, R65, W199, Y340, D366, D367, W411, K476, C526, G528, G529

(uncharacterized enzyme) with the putative ligand melibiose indicated clearly that this α-galactosidase could accommodate galactose residues in its catalytic center (Fig. 5F). This suggests a defined cavity for long chains of galacto-oligosaccharides, despite its apparent intracellular localization.

In the case of the complex AglC-stachyose modelling, the substrate adopted a position highly similar to that already observed in ligand-bound α-galactosidase from *G. stearothermophilus* (PDB ID: 4FNR) (Fig. 6A) (Merceron et al., 2012). However, an important modification in the terminal glucose and fructose binding residues was found in the AglC topology. According to the 4FNR structure, glucose of the stachyose interacts with Tyr^{340}, whereas the fructose is hydrogen-bonded to Asp^{53} and Arg^{65} to stabilize the substrate (Merceron et al., 2012). In AglC the equivalent of Tyr^{340} is Gly^{595}, but Asp^{53} and Arg^{65} are completely absent in this structure. Despite these differences, recombinant AglC is highly efficient for hydrolysis of diverse oligosaccharides, as well as to enhance the action of other galactomannanolytic enzymes to depolymerize complex polymeric substrates. It has been reported that α-galactosidases from GH36 lack the ability to release galactose from polymeric substrates, whereas they are more efficient to depolymerize small galacto-oligosaccharides (Ademark et al., 2001a; Merceron et al., 2012; Nakai et al., 2010).

Therefore, to gain insight into the possible structural determinants of the different AGLs from GH36 found in the genome of *P. subrubescens*, three structural models from the uncharacterized proteins AglH, AglK and AglM were generated for comparative modelling and used for ligand docking ensuring the high-quality of structural models (Fig. 6B–D). Whereas the other three putative proteins, corresponding to AglI, AglJ and AglL, could not be created because of low homology to any template. The ligand molecules were exactly matching the catalytic pocket of the modeled structures of AglH, AglK and AglM. In all cases, the galactose unit is stabilized in the active site by two aspartic acids (Table 4). Interestingly, the modelling analysis indicate that the structures bound to raffinose, AglH (Fig. 6B) and AglM (Fig. 6D), form a catalytic pocket that becomes wide and open to the surface. The particular conformation of these cavities in which their active sites are found, suggests a potential ability to accommodate small chains of galacto-oligosaccharides.

The observed difference in substrate specificity and molecular conformation among the rAGLs is interesting, considering that the sequences are highly homologous and use the same type of conserved residues in their catalytic mechanisms. In the future, it will be useful to evaluate what amino acid residue(s) could be the determining factor for this substrate specificity based on structural and mutational analyses, as well as find the optimal conditions to maximize the hydrolysis of galactomannan polymers by the recombinant enzymes.

4. Conclusions

This is the first report with an integral approach to identify and evaluate a complete set of α-galactosidases produced by *P. subrubescens*. Functional characterization showed that the α-galactosidases may have similar sequences but divergent substrate binding mechanisms, and in some cases, exceptional catalysis. This study provides new insights into the mechanisms underlying galactose utilization by *P. subrubescens*, and also reveals that our understanding on the hydrolysis of galactomannans is incomplete, especially because only a small fraction of GH36 fungal members have been characterized. Furthermore, these findings will contribute to improving production levels of α-galactosidases and understanding their catalytic mechanisms.

Declaration of Competing Interest

The authors declare that they have no known competing financial interests or personal relationships that could have appeared to influence the work reported in this paper.

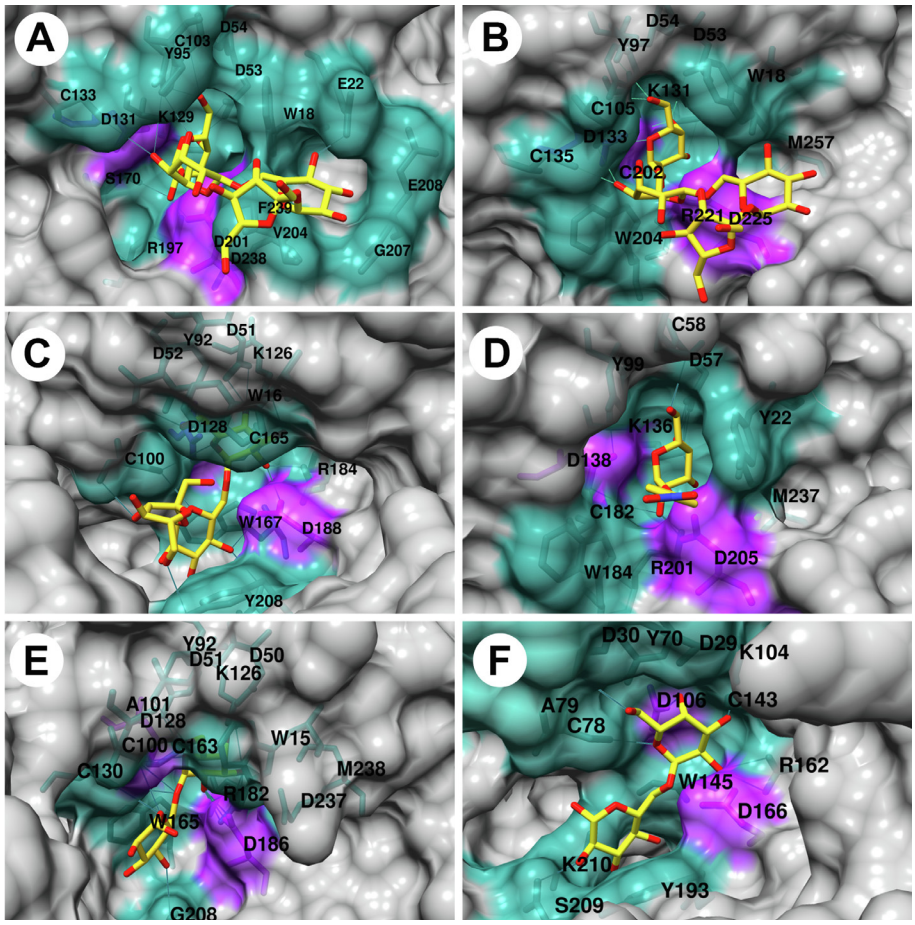

Fig. 5. 3D structural models of characterized and uncharacterized GH27 α-galactosidases from *P. subrubescens* bound with their affinity galactose-based substrates. Putative catalytic and substrate binding sites of (A) AglA with stachyose, (B) AglB with stachyose, (C) AglD with raffinose, (D) AglE with *p*NPαGal, (E) AglF with melibiose, and (F) AglG with melibiose. Galactose-based substrates are shown in yellow sticks, the catalytic residues are highlighted in purple and the putative surface binding site residues in turquoise. The hydrogen bonds formed are indicated in blue color lines. All representations were prepared using UCSF Chimera. (For interpretation of the references to color in this figure legend, the reader is referred to the web version of this article.)

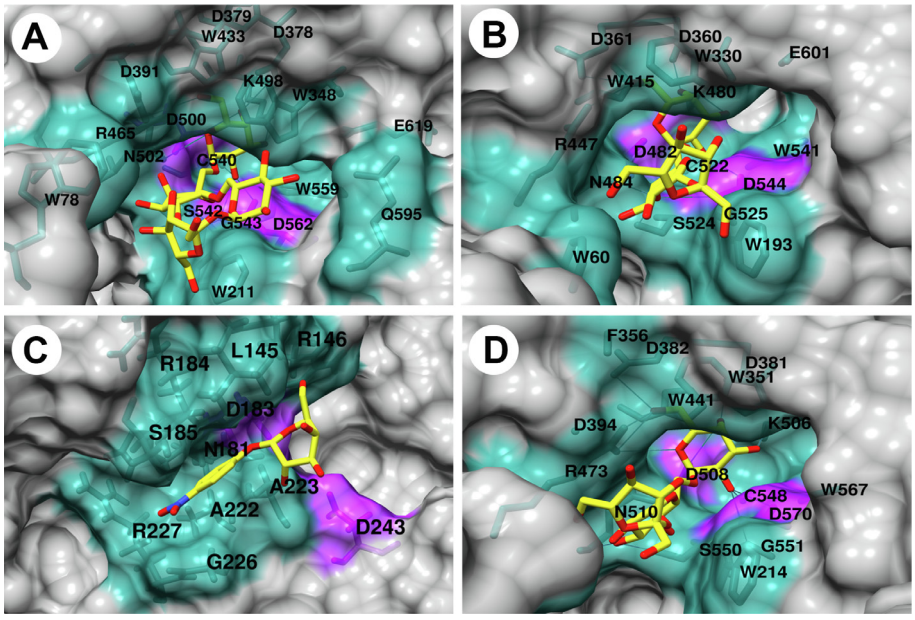

Fig. 6. 3D models of characterized and uncharacterized GH36 α-galactosidases from *P. subrubescens* with the position of galactose-based substrate ligands inside the binding site. Putative catalytic and substrate binding sites of of (A) AglC with stachyose, (B) AglH with raffinose, (C) AglK with *p*NPαGal, and (D) AglM with raffinose. Galactose-based substrate ligands are shown in yellow sticks, the catalytic residues are highlighted in purple and the putative surface binding site residues in turquoise. The hydrogen bonds formed are indicated in blue color lines. All representations were made using UCSF Chimera. (For interpretation of the references to color in this figure legend, the reader is referred to the web version of this article.)

Acknowledgements

The authors would like to thank National Council of Science and Technology of Mexico (CONACyT) for financial support (No. 263888) to NCL and the Academy of Finland (grant no. 308284) to MRM. HS thanks FORMAS and the Swedish Foundation for Strategic Research for funding.

Appendix A. Supplementary data

Supplementary data to this article can be found online at https://doi.org/10.1016/j.biortech.2019.122258.

References

Ademark, P., de Vries, R.P., Hägglund, P., Stålbrand, H., Visser, J., 2001a. Cloning and characterization of *Aspergillus niger* genes encoding an α-galactosidase and a β-mannosidase involved in galactomannan degradation. Eur. J. Biochem. 268, 2982–2990. https://doi.org/10.1046/j.1432-1327.2001.02188.x.

Ademark, P., Larsson, M., Tjerneld, F., Stålbrand, H., 2001b. Multiple α-galactosidases from *Aspergillus niger*: purification, characterization and substrate specificities. Enzyme Microb. Technol. 29, 441–448. https://doi.org/10.1016/S0141-0229(01)00415-X.

Almagro Armenteros, J.J., Tsirigos, K.D., Sønderby, C.K., Petersen, T.N., Winther, O., Brunak, S., von Heijne, G., Nielsen, H., 2019. SignalP 5.0 improves signal peptide predictions using deep neural networks. Nat. Biotechnol. 37, 420. https://doi.org/10.1038/s41587-019-0036-z.

Aulitto, M., Fusco, F.A., Fiorentino, G., Bartolucci, S., Contursi, P., Limauro, D., 2018. A thermophilic enzymatic cocktail for galactomannans degradation. Enzyme Microb. Technol. 111, 7–11. https://doi.org/10.1016/j.enzmictec.2017.12.008.

Aulitto, M., Fusco, S., Limauro, D., Fiorentino, G., Bartolucci, S., Contursi, P., 2019. Galactomannan degradation by thermophilic enzymes: a hot topic for biotechnological applications. World J. Microbiol. Biotechnol. 35, 1–13. https://doi.org/10.1007/s11274-019-2591-3.

Bauer, S., Vasu, P., Persson, S., Mort, A.J., Somerville, C.R., 2006. Development and application of a suite of polysaccharide-degrading enzymes for analyzing plant cell walls. Proc. Natl. Acad. Sci. 103, 11417–11422. https://doi.org/10.1073/pnas.0604632103.

Berka, R.M., Grigoriev, I.V., Otillar, R., Salamov, A., Grimwood, J., Reid, I., Ishmael, N., John, T., Darmond, C., Moisan, M.C., Henrissat, B., Coutinho, P.M., Lombard, V., Natvig, D.O., Lindquist, E., Schmutz, J., Lucas, S., Harris, P., Powlowski, J., Bellemare, A., Taylor, D., Butler, G., de Vries, R.P., Allijn, I.E., van den Brink, J., Ushinsky, S., Storms, R., Powell, A.J., Paulsen, I.T., Elbourne, L.D., Baker, S.E., Magnuson, J., Laboissiere, S., Clutterbuck, A.J., Martinez, D., Wogulis, M., de Leon, A.L., Rey, M.W., Tsang, A., 2011. Comparative genomic analysis of the thermophilic biomass-degrading fungi *Myceliophthora thermophila* and *Thielavia terrestris*. Nat Biotech 29, 922–927. https://doi.org/10.1038/nbt.1976.

Chen, Y., Zhang, B., Pei, H., Lv, J., Yang, W., Cao, Y., Dong, B., 2012. Directed evolution of *Penicillium janczewskii* zalesk α-galactosidase toward enhanced activity and expression in *Pichia pastoris*. Appl. Biochem. Biotechnol. 168, 638–650. https://doi.org/10.1007/s12010-012-9806-5.

Coconi Linares, N., Di Falco, M., Benoit-Gelber, I., Gruben, B.S., Peng, M., Tsang, A., Mäkelä, M.R., de Vries, R.P., 2019. The presence of trace components significantly broadens the molecular response of *Aspergillus niger* to guar gum. N. Biotechnol. 51, 57–66. https://doi.org/10.1016/j.nbt.2019.02.005.

de Vries, R.P., Burgers, K., van de Vondervoort, P.J.I., Frisvad, J.C., Samson, R.A., Visser, J., 2004. A new black *Aspergillus* species, *A. vadensis*, is a promising host for homologous and heterologous protein production. Appl. Environ. Microbiol. 70, 3954–3959. https://doi.org/10.1128/AEM.70.7.3954.

de Vries, R.P., Riley, R., Wiebenga, A., Aguilar-Osorio, G., Amillis, S., Uchima, C.A., Anderluh, G., Asadollahi, M., Askin, M., Barry, K., Battaglia, E., Bayram, Ö., Benocci, T., Braus-Stromeyer, S.A., Caldana, C., Cánovas, D., Cerqueira, G.C., Chen, F., Chen, W., Choi, C., Clum, A., dos Santos, R.A.C., Damásio, A.R. de L., Diallinas, G., Emri, T., Fekete, E., Flipphi, M., Freyberg, S., Gallo, A., Gournas, C., Habgood, R., Hainaut, M., Harispe, M.L., Henrissat, B., Hildén, K.S., Hope, R., Hossain, A., Karabika, E., Karaffa, L., Karányi, Z., Kraševec, N., Kuo, A., Kusch, H., LaButti, K., Lagendijk, E.L., Lapidus, A., Levasseur, A., Lindquist, E., Lipzen, A., Logrieco, A.F., MacCabe, A., Mäkelä, M.R., Malavazi, I., Melin, P., Meyer, V., Mielnichuk, N., Miskei, M., Molnár, Á.P., Mulé, G., Ngan, C.Y., Orejas, M., Orosz, E., Ouedraogo, J.P., Overkamp, K.M., Park, H.-S., Perrone, G., Piumi, F., Punt, P.J., Ram, A.F.J., Ramón, A., Rauscher, S., Record, E., Riaño-Pachón, D.M., Robert, V., Röhrig, J., Ruller, R., Salamov, A., Salih, N.S., Samson, R.A., Sándor, E., Sanguinetti, M., Schütze, T., Sepčić, K., Shelest, E., Sherlock, G., Sophianopoulou, V., Squina, F.M., Sun, H., Susca, A., Todd, R.B., Tsang, A., Unkles, S.E., van de Wiele, N., van Rossen-Uffink, D., Oliveira, J.V. de C., Vesth, T.C., Visser, J., Yu, J.-H., Zhou, M., Andersen, M.R., Archer, D.B., Baker, S.E., Benoit, I., Brakhage, A.A., Braus, G.H., Fischer, R., Frisvad, J.C., Goldman, G.H., Houbraken, J., Oakley, B., Pócsi, I., Scazzocchio, C., Seiboth, B., VanKuyk, P.A., Wortman, J., Dyer, P.S., Grigoriev, I. V., 2017. Comparative genomics reveals high biological diversity and specific adaptations in the industrially and medically important fungal genus Aspergillus. Genome Biol. 18, 28. doi:10.1186/s13059-017-1151-0.

de Vries, R.P., van den Broeck, H.C., Dekkers, E., Manzanares, P., de Graaff, L.H., Visser, J., 1999. Differential expression of three α-galactosidase genes and a single β-galactosidase gene from *Aspergillus niger*. Appl. Environ. Microbiol. 65, 2453–2460.

Fernández-Leiro, R., Pereira-Rodríguez, Á., Cerdán, M.E., Becerra, M., Sanz-Aparicio, J., 2010. Structural analysis of *Saccharomyces cerevisiae* α-galactosidase and its complexes with natural substrates reveals new insights into substrate specificity of GH27 glycosidases. J. Biol. Chem. 285, 28020–28033. https://doi.org/10.1074/jbc.M110.144584.

Fredslund, F., Abou Hachem, M., Jonsgaard Larsen, R., Gerd Sørensen, P., Coutinho, P.M., Lo Leggio, L., Svensson, B., 2011. Crystal structure of α-galactosidase from lactobacillus acidophilus NCFM: Insight into tetramer formation and substrate binding. J. Mol. Biol. 412, 466–480. https://doi.org/10.1016/j.jmb.2011.07.057.

Fujimoto, Z., Kaneko, S., Momma, M., Kobayashi, H., Mizuno, H., 2003. Crystal structure of rice α-galactosidase complexed with D-galactose. J. Biol. Chem. 278, 20313–20318. https://doi.org/10.1074/jbc.M302292200.

Golubev, A.M., Nagem, R.A.P., Brandão Neto, J.R., Neustroev, K.N., Eneyskaya, E.V., Kulminskaya, A.A., Shabalin, K.A., Savel'ev, A.N., Polikarpov, I., 2004. Crystal structure of α-galactosidase from Trichoderma reesei and its complex with galactose: Implications for catalytic mechanism. J. Mol. Biol. 339, 413–422. https://doi.org/10.1016/j.jmb.2004.03.062.

Hart, D.O., He, S., Chany, C.J., Withers, S.G., Sims, P.F.G., Sinnott, M.L., Brumer, H., 2000. Identification of asp-130 as the catalytic nucleophile in the main α-galactosidase from *Phanerochaete chrysosporium*, a family 27 glycosyl hydrolase. Biochemistry 39, 9826–9836. https://doi.org/10.1021/bi0008074.

Jourdier, E., Baudry, L., Poggi-Parodi, D., Vicq, Y., Koszul, R., Margeot, A., Marbouty, M., Bidard, F., 2017. Proximity ligation scaffolding and comparison of two *Trichoderma reesei* strains genomes. Biotechnol. Biofuels 10, 1–13. https://doi.org/10.1186/s13068-017-0837-6.

Kamal, S., Khan, S.U., Muhammad, N., Shoaib, M., Omar, M., Pascal, K., Rose, M.M., Sun, F.F., 2018. Insights on heterologous expression of fungal cellulases in *Pichia pastoris*. Biochem. Mol. Biol. 3, 15–35. https://doi.org/10.11648/j.bmb.20180301.13.

Katrolia, P., Rajashekhara, E., Yan, Q., Jiang, Z., 2014. Biotechnological potential of microbial α-galactosidases. Crit. Rev. Biotechnol. 34, 307–317. https://doi.org/10.3109/07388551.2013.794124.

Kumar, S., Stecher, G., Tamura, K., 2016. MEGA7: Molecular Evolutionary Genetics Analysis version 7.0 for bigger datasets. Mol. Biol. Evol. 33, 1870–1874. https://doi.org/10.1093/molbev/msw054.

Kurakake, M., Moriyama, Y., Sunouchi, R., Nakatani, S., 2011. Enzymatic properties and transglycosylation of α-galactosidase from *Penicillium oxalicum* SO. Food Chem. 126, 177–182. https://doi.org/10.1016/j.foodchem.2010.10.095.

Kytidou, K., Beekwilder, J., Artola, M., van Meel, E., Wilbers, R.H.P., Moolenaar, G.F., Goosen, N., Ferraz, M.J., Katzy, R., Voskamp, P., Florea, B.I., Hokke, C.H., Overkleeft, H.S., Schots, A., Bosch, D., Pannu, N., Aerts, J.M.F.G., 2018. *Nicotiana benthamiana* α-galactosidase A1.1 can functionally complement human α-galactosidase A deficiency associated with Fabry disease. J. Biol. Chem. 293, 10042–10058. https://doi.org/10.1074/jbc.RA118.001774.

Laskowski, R.A., Rullmann, J.A.C., MacArthur, M.W., Kaptein, R., Thornton, J.M., 1996. AQUA and PROCHECK-NMR: programs for checking the quality of protein structures solved by NMR. J. Biomol. NMR 8, 477–486.

Liao, J., Okuyama, M., Ishihara, K., Yamori, Y., Iki, S., Tagami, T., Mori, H., Chiba, S., Kimura, A., 2016. Kinetic properties and substrate inhibition of α-galactosidase from *Aspergillus niger*. Biosci. Biotechnol. Biochem. 8451, 1–6. https://doi.org/10.1080/09168451.2015.1136884.

Lombard, V., Golaconda Ramulu, H., Drula, E., Coutinho, P.M., Henrissat, B., 2014. The carbohydrate-active enzymes database (CAZy) in 2013. Nucleic Acids Res. 42, 490–495. https://doi.org/10.1093/nar/gkt1178.

Luonteri, E., Alatalo, E., Siika-Aho, M., Penttilä, M., Tenkanen, M., 1998a. α-galactosidases of *Penicillium simplicissimum*: production, purification and characterization of the gene encoding AGLI. Biotechnol. Appl. Biochem. 28, 179–188. https://doi.org/10.1111/j.1470-8744.1998.tb00528.x.

Luonteri, E., Tenkanen, M., Viikari, L., 1998b. Substrate specificities of penicillium simplicissimum α-galactosidases. Enzyme Microb. Technol. 22, 192–198. https://doi.org/10.1016/S0141-0229(97)00170-1.

Malgas, S., Thoresen, M., van Dyk, J.S., Pletschke, B.I., 2017. Time dependence of enzyme synergism during the degradation of model and natural lignocellulosic substrates. Enzyme Microb. Technol. 103, 1–11. https://doi.org/10.1016/j.enzmictec.2017.04.007.

Malgas, S., van Dyk, S.J., Pletschke, B.I., 2015. β-Mannanase (Man26A) and α-galactosidase (Aga27A) synergism – A key factor for the hydrolysis of galactomannan substrates. Enzyme Microb. Technol. 70, 1–8. https://doi.org/10.1016/j.enzmictec.2014.12.007.

Merceron, R., Foucault, M., Haser, R., Mattes, R., Watzlawick, H., Gouet, P., 2012. The molecular mechanism of thermostable α-galactosidases AgaA and AgaB explained by X-ray crystallography and mutational studies. J. Biol. Chem. 287, 39642–39652. https://doi.org/10.1074/jbc.M112.394114.

Mi, S., Meng, K., Wang, Y., Bai, Y., Yuan, T., Luo, H., Yao, B., 2007. Molecular cloning and characterization of a novel α-galactosidase gene from *Penicillium* sp. F63 CGMCC 1669 and expression in *Pichia pastoris*. Enzyme Microb. Technol. 40, 1373–1380. https://doi.org/10.1016/j.enzmictec.2006.10.017.

Morales-Quintana, L., Faúndez, C., Herrera, R., Zavaleta, V., Ravanal, M.C., Eyzaguirre, J., Moya-León, M.A., 2017. Biochemical and structural characterization of *Penicillium purpurogenum* α-D galactosidase: Binding of galactose to an alternative pocket may explain enzyme inhibition. Carbohydr. Res. 448, 57–66. https://doi.org/10.1016/j.carres.2017.05.020.

Nakai, H., Baumann, M.J., Petersen, B.O., Westphal, Y., Hachem, M.A., Dilokpimol, A., Duus, J.O., Schols, H.A., Svensson, B., 2010. *Aspergillus nidulans* α-galactosidase of glycoside hydrolase family 36 catalyses the formation of α-galacto-oligosaccharides by transglycosylation. FEBS J. 277, 3538–3551. https://doi.org/10.1111/j.1742-4658.2010.07763.x.

Naumoff, D.G., 2011. Hierarchical classification of glycoside hydrolases. Biochem. 76, 622–635. https://doi.org/10.1134/s0006297911060022.

Naumoff, D.G., 2004. Phylogenetic analysis of α-galactosidases of the GH27 family. Mol. Biol. 38, 388–399.

Peng, M., Dilokpimol, A., Mäkelä, M.R., Hildén, K., Bervoets, S., Riley, R., Grigoriev, I.V., Hainaut, M., Henrissat, B., de Vries, R.P., Granchi, Z., 2017. The draft genome sequence of the ascomycete fungus *Penicillium subrubescens* reveals a highly enriched content of plant biomass related CAZymes compared to related fungi. J. Biotechnol. 246, 1–3. https://doi.org/10.1016/j.jbiotec.2017.02.012.

Pettersen, E.F., Goddard, T.D., Huang, C.C., Couch, G.S., Greenblatt, D.M., Meng, E.C., Ferrin, T.E., 2004. UCSF Chimera – A visualization system for exploratory research and analysis. J. Comput. Chem. 25, 1605–1612. https://doi.org/10.1002/jcc.20084.

Prlić, A., Bliven, S., Rose, P.W., Bluhm, W.F., Bizon, C., Godzik, A., Bourne, P.E., 2010. Pre-calculated protein structure alignments at the RCSB PDB website. Bioinformatics 26, 2983–2985. https://doi.org/10.1093/bioinformatics/btq572.

Sakamoto, T., Tsujitani, Y., Fukamachi, K., Taniguchi, Y., Ihara, H., 2010. Identification of two GH27 bifunctional proteins with β-L- arabinopyranosidase/α-D-galactopyranosidase activities from *Fusarium oxysporum*. Appl. Microbiol. Biotechnol. 86, 1115–1124. https://doi.org/10.1007/s00253-009-2344-6.

Sinitsyna, O.A., Fedorova, E.A., Vakar, E., Semenova, M.V., Gusakov, A.V., Sokolova, L.M., Bubnova, T.M., Okunev, O.N., Chulkin, A.M., Vavilova, E.A., Vinetsky, Y.P., Sinitsyn, A.P., 2008. Isolation and characterization of extracellular α-galactosidases from from *Penicillium canescens*. Biochem. 73, 97–106. https://doi.org/10.1134/S0006297907050148.

Song, Y., Sun, W., Fan, Y., Xue, Y., Liu, D., Ma, C., Liu, W., Mosher, W., Luo, X., Li, Z., Ma, W., Zhang, T., 2018. Galactomannan degrading enzymes from the mannan utilization gene cluster of alkaliphilic *Bacillus sp.* N16–5 and their synergy on galactomannan degradation. J. Agric. Food Chem. 66, 11055–11063. https://doi.org/10.1021/acs.jafc.8b03878.

Vesth, T.C., Nybo, J.L., Theobald, S., Frisvad, J.C., Larsen, T.O., Nielsen, K.F., Hoof, J.B., Brandl, J., Salamov, A., Riley, R., Gladden, J.M., Phatale, P., Nielsen, M.T., Lyhne, E.K., Kogle, M.E., Strasser, K., McDonnell, E., Barry, K., Clum, A., Chen, C., LaButti, K., Haridas, S., Nolan, M., Sandor, L., Kuo, A., Lipzen, A., Hainaut, M., Drula, E., Tsang, A., Magnuson, J.K., Henrissat, B., Wiebenga, A., Simmons, B.A., Mäkelä, M.R., de Vries, R.P., Grigoriev, I.V., Mortensen, U.H., Baker, S.E., Andersen, M.R., 2018. Investigation of inter- and intraspecies variation through genome sequencing of *Aspergillus* section *Nigri*. Nat. Genet. 50, 1688–1695. https://doi.org/10.1038/s41588-018-0246-1.

Wallner, B., Fang, H., Elofsson, A., 2003. Automatic consensus-based fold recognition using Pcons, ProQ, and Pmodeller. Proteins Struct. Funct. Genet. 53, 534–541. https://doi.org/10.1002/prot.10536.

Wang, H., Ma, R., Shi, P., Huang, H., Yang, P., Wang, Y., Fan, Y., Yao, B., 2014. Insights into the substrate specificity and synergy with mannanase of family 27 α-galactosidases from *Neosartorya fischeri* P1. Appl. Microbiol. Biotechnol. 99, 1261–1272. https://doi.org/10.1007/s00253-014-6269-3.

Wiederstein, M., Sippl, M.J., 2007. ProSA-web: interactive web service for the recognition of errors in three-dimensional structures of proteins. Nucleic Acids Res. 35, 407–410. https://doi.org/10.1093/nar/gkm290.

Zeilinger, S., Kristufek, D., Arisan-Atac, I., Hodits, R., Kubicek, C.P., 1993. Conditions of formation, purification, and characterization of an α-galactosidase of *Trichoderma reesei* RUT C-30. Appl. Environ. Microbiol. 59, 1347–1353.

Zheng, X., Fang, B., Han, D., Yang, W., Qi, F., Chen, H., Li, S., 2016. Improving the secretory expression of an α-galactosidase from *Aspergillus niger* in *Pichia pastoris*. PLoS One 11, 1–12. https://doi.org/10.1371/journal.pone.0161529.